Smart Structures and Systems, *Vol. 25, No. 2 (2020) 255-264*
DOI: https://doi.org/10.12989/sss.2020.25.2.255

Defect classification of refrigerant compressor using variance estimation of the transfer function between pressure pulsation and shell acceleration

Yeon-Woo Kim [a] and Weui-Bong Jeong*

Department of Mechanical Engineering, Pusan National University, Jangjeon-dong, Kumjung-gu, Busan 609-735, Republic of Korea

(*Received Feburary 28, 2019, Revised May 27, 2019, Accepted June 20, 2019*)

Abstract. This paper deals with a defect classification technique that considers the structural characteristics of a refrigerant compressor. First, the pressure pulsation of the refrigerant flowing in the suction pipe of a normal compressor was measured at the same time as the acceleration of the shell surface, and then the transfer function between the two signals was estimated. Next, the frequency-weighted acceleration signals of the defect classification target compressors were generated using the estimated transfer function. The estimation of the variance of the transfer function is presented to formulate the frequency-weighted acceleration signals. The estimated frequency-weighted accelerations were applied to defect classification using frequency-domain features. Experiments were performed using commercial compressors to verify the technique. The results confirmed that it is possible to perform an effective defect classification of the refrigerant compressor by the shell surface acceleration of the compressor. The proposed method could make it possible to improve the total inspection performance for compressors in a mass-production line.

Keywords: defect classification; linear compressor; transfer function; frequency analysis; variance minimize; mass-production inspection; FDR

1. Introduction

Compressors have very important roles in daily life. Small refrigerant compressors are used in air conditioners or refrigerators, where failure can have a big influence on the brand value of the product. Therefore, compressor manufacturers are paying much attention to fault diagnosis techniques to improve their brand value.

Various studies have been conducted on fault diagnosis and defect detection for compressors. Mathioudakis and Stamatis (1994) and Kim and Kim (2005) proposed methods of detecting defects in a compressor by using experimental data in varying operating conditions. Aretakis and Mathioudakis (1998) proposed a method of fault diagnosis by analyzing the signal pattern of the sound emission and casing vibration of a compressor. Elhaj *et al.* (2008) simulated the behavior of the valves of compressors and proposed a fault diagnosis technique based estimation of the cylinder pressure waveforms and instantaneous angular speed of the crankshaft.

Cui *et al.* (2009) proposed a compressor fault diagnosis technique using the estimated entropy from the acceleration signal of a compressor. Zhu *et al.* (2010) and Jung and Koh (2014) proposed a fault diagnosis method for a reciprocating motion device using a wavelet transform. Althobiami and Ball (2014) proposed a fault diagnosis technique for a compressor using the wavelet of pressure and acceleration signals of industrial air compressors. Wang *et al.* (2015) estimated the behavior of a compressor valve from the radiated noise on the surface of a compressor and proposed a fault diagnosis based on the derived signals. Pichler *et al.* (2016) proposed a technique for the classification of compressor valve defects using a two-dimensional autocorrelation of the radiated noise of a compressor while controlling the load.

There are many studies on techniques for compressor fault diagnosis based on artificial neural networks (ANN) or big data. Yang *et al.* (2005) performed fault diagnosis using small refrigerant compressors using supported vector machine (SVM) and ANN. Zhou *et al.* (2006) performed fault diagnosis using ANN and entropy change of compressor vibration signal. Shen *et al.* (2014) and Fan *et al.* (2015) proposed fault diagnosis techniques in which a machine learns and classifies various signals from a compressor by using ANN. Qi *et al.* (2016, 2018), Tran *et al.* (2017) proposed pattern analysis methods for big data that analyze the vast amount of data from various compressor signals and find the pattern of fault signals. Ouadine *et al.* (2018) studied an optimization technique for compressor fault diagnosis using an artificial neural network and genetic algorithm. Loukopoulos *et al.* (2019) proposed a technique for predicting the potential failure of a compressor valve based on big data. However, most of these studies do not take into account the complex environment in an actual mass-production line for compressors since they use signals measured in a controlled laboratory environment.

In general, the refrigerant pressure pulsation signal in the suction pipe is used to diagnose a potential failure or defect of a compressor for a refrigerator. The refrigerant

*Corresponding author, Ph.D., Professor,
E-mail: wbjeong@pusan.ac.kr
[a] Ph.D. Candidate

Copyright © 2020 Techno-Press, Ltd.
http://www.techno-press.org/?journal=sss&subpage=7
ISSN: 1738-1584 (Print), 1738-1991 (Online)

pressure pulsation is most affected by compressor failure, and techniques that use this signal are very intuitive and highly reliable. However, to measure the pulsation, it is necessary to stabilize the refrigerant after filling and sealing it in the compressor. It is difficult to apply this to a mass-production line since additional work is required, such as inserting a pressure sensor into the piping. Therefore, many compressor manufacturers are conducting full-scale compressor inspections on mass-production lines using acceleration signals from the surface of a relatively easy-to-measure compressor shell.

However, in the case of the acceleration signal on the compressor shell surface, the behavior of the compressor's suction valve and the structural characteristics of the compressor are simultaneously measured, which is not suitable for direct use in failure determination. Therefore, compressor manufacturers diagnose compressor defects using the amplitude change of the peak of a specific frequency band through signal processing. However, the remaining structural characteristics of the compressor are not removed, so the defect detection rate is not satisfactory. To solve these issues, Kim and Jeong (2019) proposed a defect detection technique using the transfer function between the refrigerant pressure pulsation and the shell surface acceleration in the suction pipe of the compressor using the Total Least-Squares (TLS) method. However, additional signal processing for raw data was required to estimate the variance of the measured signal in the previous paper. In order to overcome this difficulty, a new signal processing using the coherence function is presented in this paper. The coherence function can be easily obtained in signal measurement.

In the present study, the relationship between the refrigerant pressure pulsation and the shell surface acceleration is expressed as a transfer function. The acceleration signal is weighted since it is easy to measure. A technique is proposed for minimizing the variance of the transfer function in the frequency domain and was confirmed by experiments. We also propose a defect classification method that is suitable for full-scale inspection of compressors in the mass production process and has excellent performance.

2. Theory

2.1 Frequency-weighted transfer function

The opening and closing movements of the suction valve result in pressure pulsation of the refrigerant in the suction pipe and acceleration of the compressor shell surface. The pulsation signal is directly affected by the behavior of the suction valve, so it is advantageous for defect classification but is difficult to measure directly. However, the measured acceleration signal includes the structural characteristics of the compressor and the influence of pipe vibration and is easy to measure. Therefore, it is desirable to use the transfer function between the refrigerant pressure pulsation and shell acceleration to improve the defect classification performance of the shell acceleration signal. The schematic of acquired signals by suction valve movement are shown in Fig. 1.

Let H(f) be the transfer function between the refrigerant pressure pulsation of the compressor piping (the input signal) and the acceleration of the compressor surface (the output signal). The true value of the pulsation applied to the delivery path is u(t), but the value p(t) measured by the pressure transducer contains input noise m(t). Similarly, the measured output value a(t) of the shell surface acceleration transducer at the output stage also includes output noise n(t) in the true value v(t). The relationship between the pulsation and acceleration is shown in Eq. (1) and Fig. 2 (Shin and Hammond 2008).

$$\begin{aligned} p(t) &= u(t) + m(t) \\ a(t) &= v(t) + n(t) \end{aligned} \tag{1}$$

$H_1(f)$ and $H_2(f)$ are transfer functions that are widely used in industrial applications and are defined as follows.

$$\begin{aligned} H_1(f) &= \frac{S_{pa}(f)}{S_{pp}(f)} \\ H_2(f) &= \frac{S_{aa}(f)}{S_{ap}(f)} \end{aligned} \tag{2}$$

Where $S_{pa}(f)$ is the cross-spectral density of a(t) and p(t), and $S_{pp}(f)$ and $S_{aa}(f)$ are auto-spectral density functions of a(t) and p(t).

$H_1(f)$ converges to the true value $H_{true}(f)$ when there is only input noise, and $H_2(f)$ converges to the true value $H_{true}(f)$ when there is only output noise. The true transfer function $H_{true}(f)$ between $H_1(f)$ and $H_2(f)$ exists when there is noise in both the input and output, which can be represented as follows.

$$H_1(f) \leq H_{true}(f) \leq H_2(f) \tag{3}$$

The coherence function is widely used as a measure of

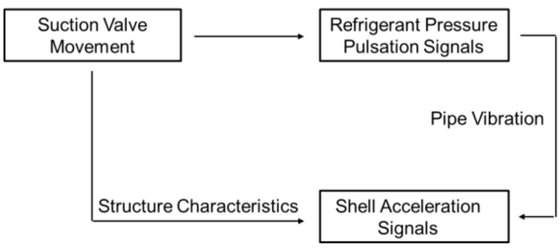

Fig. 1 Schematic of acquired signals by suction valve movement

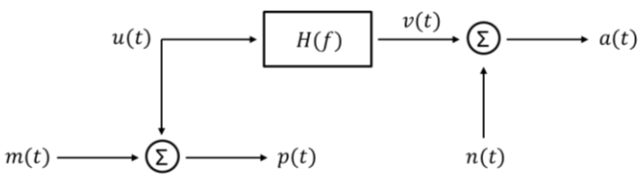

Fig. 2 Schematic of single input-output system with extraneous noise

the degree of correlation between input and output signals of a linear system in the frequency domain (Bendat and Piersol 1980)

$$\gamma_{pa}^2(f) = \frac{\left|S_{pa}(f)\right|^2}{S_{pp}(f)S_{aa}(f)}, \quad 0 \le \gamma_{pa}^2(f) \le 1 \tag{4}$$

The following relation holds between the power spectrum $S_{pp}(f)$ of the pulsation signal and the power spectrum $S_{aa}(f)$ of the acceleration signal.

$$S_{pp}(f) = \frac{S_{aa}(f)}{|H(f)|^2} \tag{5}$$

Assuming that the estimated value of the transfer function $|H(f)|$ is normally distributed with respect to the true value $|H_{true}(f)|$, the probability density function $p(|H(f)|)$ at which the transfer function $|H(f)|$ is obtained is as follows.

$$p(|H(f)|) = \frac{1}{\sqrt{2\pi}\sigma_H(f)} e^{-\frac{[|H(f)|-E[|H(f)|]]^2}{2\sigma_H^2(f)}} \tag{6}$$

The value of $|H(f)|$ is highly in reliable in a frequency band where the variance $\sigma_H^2(f)$ is small, but the reliability is low when the variance is large. Therefore, the transfer function for defect classification is defined as follows in consideration of the frequency weighting.

$$S_{aa.weighted}(f) = \frac{S_{aa}(f)}{\frac{1}{\sigma_H^2(f)}|H(f)|^2} \tag{7}$$

Here, the transfer function $H(f)$ means $H_1(f)$ or $H_2(f)$, and the estimation method of the variance $\sigma_H^2(f)$ is given in the next section.

2.2 Estimation of the transfer function variance

Fig. 2 shows the relations of $P(f) = U(f) + M(f)$, $V(f)$ $H_{rue}(f)U(f)$, and $A(f) = V(f) + N(f)$. The input noise $M(f)$ and the output noise $N(f)$ are assumed to be uncorrelated with the signals $U(f)$ and $V(f)$. Thus, $S_{um}(f)$, $S_{vm}(f)$, $S_{un}(f)$, $S_{un}(f)$, $S_{vn}(f)$, and $S_{mn}(f)$ are all zero (Shin and Hammond 2008).

The value of the transfer function $H_i(f)$ sampled at the i-th measurement is a random variable and can be expressed as follows.

$$H_i(f) = \frac{V(f) + N_i(f)}{U(f) + M_i(f)} \tag{8}$$

Assuming that noise and signal are uncorrelated and $M(f)/U(f)$ and $N(f)/V(f)$ are sufficiently small, the ensemble-averaged value of H (f) can be expressed as follows.

$$\begin{aligned} E[H(f)] &= \lim_{N\to\infty}\frac{1}{N}\sum_{i=1}^{N} H_i(f) \\ &= \lim_{N\to\infty}\frac{1}{N}\sum_{i=1}^{N}\frac{V(f)}{U(f)}\left(1+\frac{N_i(f)}{V(f)}\right)\left(\begin{matrix}1+\dfrac{M_i(f)}{V(f)} \\ +\text{higher order}\end{matrix}\right) \\ &\approx H_{true}(f) \end{aligned} \tag{9}$$

$|H_i(f)|^2$ can be expressed as follows.

$$\begin{aligned} &H_i^*(f)H_i(f) \\ &= \frac{V^*(f)V(f) + V^*(f)N_i(f) + N_i^*(f)V(f) + N_i^*(f)N_i(f)}{U^*(f)U(f) + U^*(f)M_i(f) + M_i^*(f)U(f) + M_i^*(f)M_i(f)} \end{aligned} \tag{10}$$

The ensemble-averages value of $|H_i(f)|^2$ can be expressed as follows.

$$\begin{aligned} E[|H(f)|^2] &= \lim_{N\to\infty}\frac{1}{N}\sum_{i=1}^{N} H_i^*(f)H_i(f) \\ &= \lim_{N\to\infty}\frac{1}{N}\sum_{i=1}^{N}\frac{V_i^*(f)V(f)_i}{U_i^*(f)U_i(f)}\left(\frac{1+\frac{N_i(f)}{V(f)}+\frac{N_i^*(f)}{V^*(f)}+\frac{N_i^*(f)N_i(f)}{V^*(f)V(f)}}{1+\frac{M_i(f)}{U(f)}+\frac{M_i^*(f)}{U^*(f)}+\frac{M_i^*(f)M_i(f)}{U^*(f)U(f)}}\right) \\ &= H_{true}^*(f)H_{true}(f)\lim_{N\to\infty}\frac{1}{N}\sum_{i=1}^{N}\left[1+\frac{N_i^*(f)N_i(f)}{V^*(f)V(f)}\right] \\ &\quad\left[\begin{matrix}1-\left(\frac{M_i(f)}{U(f)}+\frac{M_i^*(f)}{U^*(f)}+\frac{M_i^*(f)M_i(f)}{U^*(f)U(f)}\right) \\ +\left(\frac{M_i(f)}{U(f)}+\frac{M_i^*(f)}{U^*(f)}+\frac{M_i^*(f)M_i(f)}{U^*(f)U(f)}\right)^2 + \text{higher order}\end{matrix}\right] \\ &= H_{true}^*(f)H_{true}(f)\left(1+\frac{S_{nn}(f)}{S_{vv}(f)}\right)\left(1-\frac{S_{mm}(f)}{S_{uu}(f)}\right. \\ &\quad\left.+\lim_{N\to\infty}\frac{1}{N}\sum_{i=1}^{N}\left[\left(\frac{M_i(f)}{U(f)}+\frac{M_i^*(f)}{U^*(f)}\right)^2\right]+\text{higher order}\right) \\ &= H_{true}^*(f)H_{true}(f)\left(1+\frac{S_{nn}(f)}{S_{vv}(f)}\right)\left(1-\frac{S_{mm}(f)}{S_{uu}(f)}\right. \\ &\quad+\lim_{N\to\infty}\frac{1}{N}\sum_{i=1}^{N}\left[\frac{4(M_{R,i}^2(f)U_R^2(f)+M_{I,i}^2(f)U_I^2(f))}{(U_R^2(f)+U_I^2(f))}\right] \\ &\quad\left.+\text{higher order}\right) \end{aligned} \tag{11}$$

The subscripts R and I represent the real and imaginary parts of a complex number.

The spectrum of the input noise is denoted by $M(f) = M_R(f) + jM_I(f)$, and the expected values of the real and imaginary parts of the random noise are stochastically the same.

$$E[M_R^2(f)] = E[M_I^2(f)] = E\left[\frac{1}{2}M^*(f)M(f)\right] \tag{12}$$

Therefore, Eq. (11) can be expressed as follows.

$$\begin{aligned} E[|H(f)|^2] &= H_{true}^*(f)H_{true}(f)\left(1+\frac{S_{nn}(f)}{S_{vv}(f)}\right)\left(1-\frac{S_{mm}(f)}{S_{uu}(f)}\right. \\ &\quad\left.+\lim_{N\to\infty}\frac{1}{N}\sum_{i=1}^{N}\left(\begin{matrix}\left[\dfrac{2\left(M_i^*(f)M_i(f)U^*(f)U(f)\right)}{\left(U^*(f)U(f)\right)^2}\right] \\ +\text{higher order}\end{matrix}\right)\right) \\ &\approx H_{true}^*(f)H_{true}(f)\left(1+\frac{S_{nn}(f)}{S_{vv}(f)}\right)\left(1+\frac{S_{mm}(f)}{S_{uu}(f)}\right) \end{aligned} \tag{13}$$

Assuming the input noise m(t) is zero, the transfer function H_1 is $E[|H_1(f)|^2] = |H_{true}(f)|^2(1 + S_{nn}(f)/S_{vv}(f))$, regardless of the magnitude of the signal-to-noise ratio (SNR).

The transfer function H_2 is assumed to have output noise $n(t) = 0$ and can be approximated as $E[|H_2(f)|^2] \approx |H_{true}(f)|^2(1 + S_{mm}(f)/S_{uu}(f))$ when the SNR is sufficiently small.

The coherence function of Eq. (4) can be expressed as follows.

$$\begin{aligned} \gamma_{pa}^2(f) &= \frac{\left|S_{pa}(f)\right|^2}{S_{pp}(f)S_{aa}(f)} = \frac{\left|H_{true}(f)\right|^2 S_{uu}^2(f)}{[S_{uu}(f)+S_{mm}(f)][S_{vv}(f)+S_{nn}(f)]} \\ &= \frac{\left|H_{true}(f)\right|^2 S_{uu}^2(f)}{S_{uu}(f)\left(1+\frac{S_{mm}(f)}{S_{uu}(f)}\right)S_{vv}(f)\left(1+\frac{S_{nn}(f)}{S_{vv}(f)}\right)} \end{aligned} \tag{14}$$

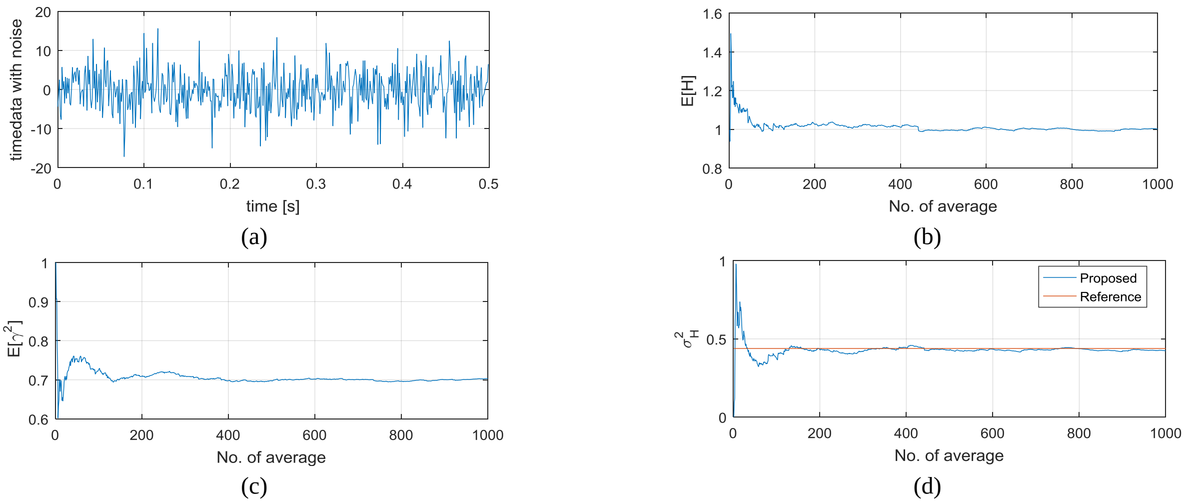

Fig. 3 Validation of Eq. (15): (a) Time data with noise; (b) $E[H(f_0)]$ versus average number; (c) $E[\gamma^2(f_0)]$ versus average number; (d) $\sigma_H^2(f_0)$ versus average number

$$= \frac{|H_{true}(f)|^2}{|H_{true}(f)|^2\left(1+\frac{S_{mm}(f)}{S_{uu}(f)}\right)\left(1+\frac{S_{nn}(f)}{S_{vv}(f)}\right)} = \frac{|E[H(f)]|^2}{E[|H(f)|^2]} \tag{14}$$

Thus, the variance $\sigma_H^2(f)$ of the estimate of H(f) can be expressed as the coherence function and the magnitude of the transfer function as follows.

$$\begin{aligned}\sigma_H^2(f) &= E\left[|H(f)|^2\right] - |E[H(f)]|^2 \\ &\approx \frac{1-\gamma_{pa}^2(f)}{\gamma_{pa}^2(f)}|E[H(f)]|^2\end{aligned} \tag{15}$$

Therefore, the power spectrum of the frequency-weighted acceleration signal using H(f) given in Eq. (7) is obtained as follows.

$$S_{aa,weighted}(f) = \frac{1-\gamma_{pa}^2(f)}{\gamma_{pa}^2(f)}\frac{1}{|H(f)|^2}S_{aa}(f) \tag{16}$$

2.3 Validation

In Fig. 2, the true values of the transfer function and the input signal can be assumed to be H(f) = 1 and $u(t) = \sin(2\pi f_0 t)$, respectively. Therefore, the measured input signal and output signal can be represented by $p(t) = \sin(2\pi f_0 t) + m(t)$ and $a(t) = \sin(2\pi f_0 t) + n(t)$, respectively, where $f_0 = 6$ Hz and m(t) and n(t) are normally distributed white noise.

An example of a time signal with white noise is shown in Fig. 3(a).

Figs. 3(b) and (c) show the transfer function and coherence function γ_{pa}^2 according to the average number of in $f = f_0$ Hz. As the average number increases, the transfer function converges to the initial set value of 1 and γ_{pa}^2 converges to about 0.7024. Fig. 3(d) shows the variance of the transfer function according to the average number, which converged to about 0.4237. The convergence value was found to match the value of $E[H_i(f)] = 1$ and $\gamma_{pa}^2 = 0.7024$ in the approximate expression of $\sigma_H^2(f)$ in Eq. (15), which validates the proposed expression.

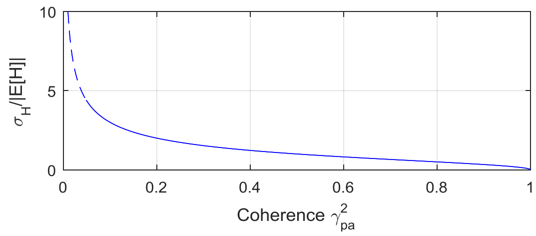

Fig. 4 Normalized deviation of transfer function versus coherence function

The normalized deviation of the transfer function is a dimensionless form of Eq. (15) and expressed as follows.

$$\frac{\sigma_H(f)}{|E[H(f)]|} \approx \sqrt{\frac{1-\gamma_{pa}^2(f)}{\gamma_{pa}^2(f)}} \tag{17}$$

Fig. 4 shows the normalized deviation of the transfer function $\sigma_H/|E[H]|$ according to the magnitude of the coherence function γ_{pa}^2.

When $\gamma_{pa}^2(f_0) \rightarrow 0$, $\sigma_H/E|[H(f_0)]| \rightarrow \infty$, and when $\gamma_{pa}^2(f_0) \rightarrow 1$, $\sigma_H/|E[H(f_0)]| \rightarrow 0$.

3. Application to defect classification of refrigerant compressor

3.1 Experimental overview

Experiments were carried out with actual compressors to verify the fault classification performance of the frequency-weighted acceleration signal. In this study, a linear compressor with 34 kWh/month power consumption is applied. This compressor is usually used for the household refrigerator with 870 L capacity. The pressure pulsation of the refrigerant flowing into the pipe was measured by a pressure sensor that was inserted vertically into the

Table 1 Defect information of the compressor used in the experiment

Defect No.	Cause of defect	Excess amount of noise compared to manufacturer's standard value
Defect 1	Defect on inner bearing	0.1 dB
Defect 2	Defect on assembly	1.8 dB
Defect 3	Compressor's internal pressure exceeded	5.9 dB

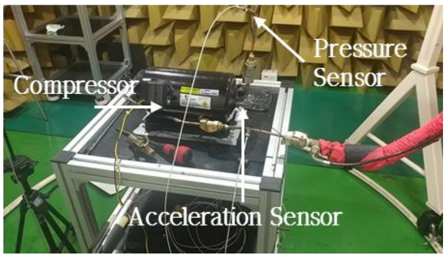

Fig. 5 Refrigerant supply system in anechoic chamber

refrigerant suction pipe of the compressor. The acceleration of the shell surface was measured by an acceleration sensor that was attached to the center of the compressor.

One normal compressor and three compressors with different defects were used in the experiment. The defective compressors were defective products that had been returned after actually being sold. Noise tests were conducted, which confirmed that the noise level of the defective compressor exceeded the noise specifications from the manufacturer. The cause of the defects and the amount of excess noise are listed in Table 1.

The refrigerant circulation cycle of the refrigerator compressor differs according to the operating procedure and refrigerator settings. Therefore, even if the same compressor is used in the experiment, the results may vary with the operating conditions and the refrigerator model. To prevent this situation, the refrigerant supply system was installed in an anechoic chamber with vibration insulation, as shown Fig. 5. The refrigerant circulation cycle of the actual refrigerator was kept constant, the external vibration noise was minimized through the vibration insulation, and several compressors were tested under the same conditions.

LMS Test.Lab equipment was used to obtain the experimental data. The pressure sensor was a KISTLER 211B3 model, and the acceleration sensor was Bruel & Kjaer A397 model. The suction pipe refrigerant pressure pulsation and the compressor surface acceleration data were acquired for 60 seconds at intervals of 4.88×10^{-5} seconds. A compressor operating frequency of 80 Hz was applied, which is the actual value of the compressor model used in the experiment.

Some of the experimental data obtained from the experiment are shown in Figs. 6 and 7.

Figs. 6(a) and (b) show that the compressor's operating frequency of 80 Hz is strongly measured in the pressure pulse signals of all products. Fig. 6(b) shows that the base level of the normal product is significantly lower than that of the defective products except for the peak in the entire frequency band. In addition, the peak of electric noise occurs at 60 Hz. Fig. 7(a) shows that a strong high-frequency signal appears in the shell surface acceleration of all products. In Fig. 7(b), the electric noise found at 60 Hz in Fig. 6(b) is relatively weak. There is no large difference in the base level except for the peak in the entire frequency band.

Figs. 6 and 7 show that both the refrigerant pressure

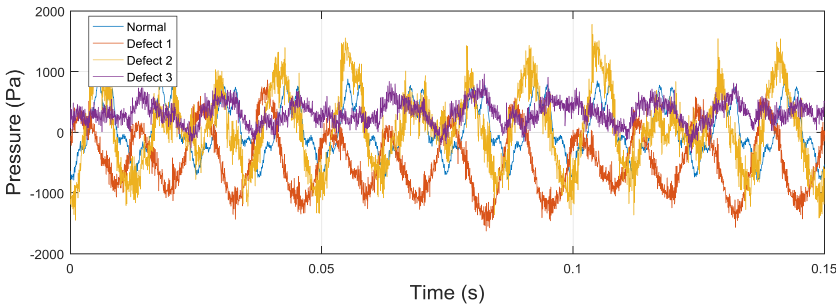

(a)

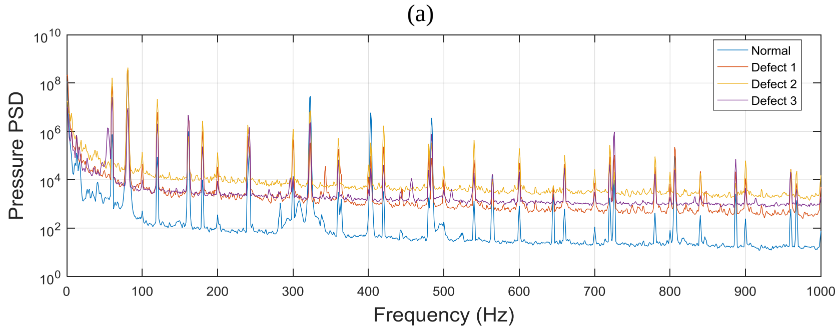

(b)

Fig. 6 Pressure pulsation signal measured in the experiment: (a) Time domain data; (b) Frequency domain data

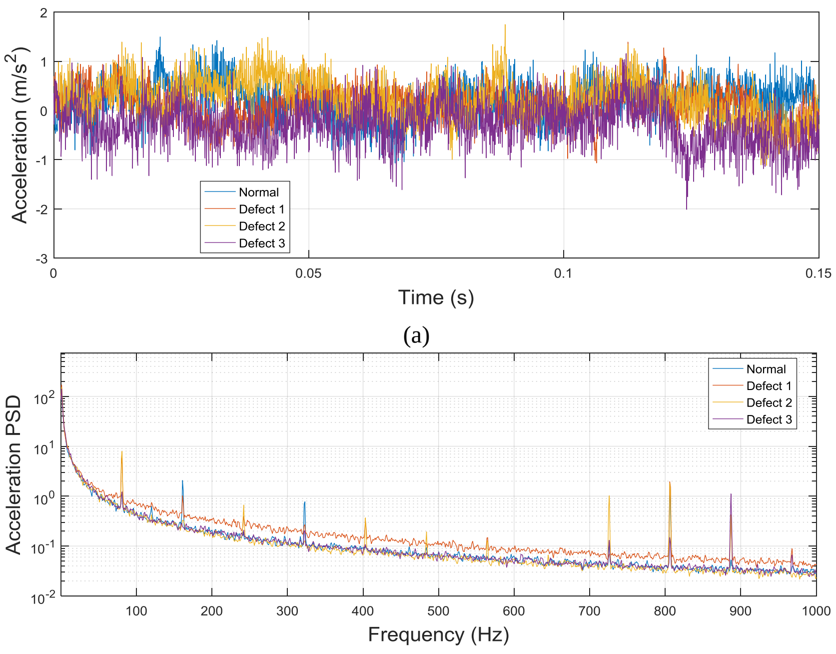

(b)

Fig. 7 Shell acceleration signal measured in the experiment: (a) Time domain data; (b) Frequency domain data

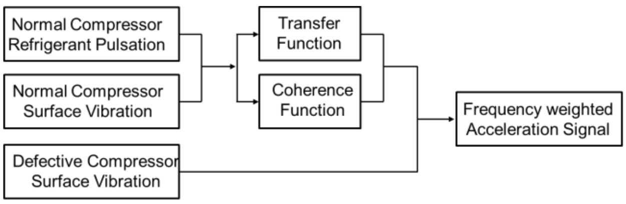

Fig. 8 Schematic of estimating the frequency-weighted acceleration signal

pulsation signal and the shell surface acceleration signal generate a large peak at the operating frequency of 80 Hz and the harmonics. Furthermore, the refrigerant pressure pulsation signal shows that the signal characteristics of the defective product are distinct from that of the normal product. The refrigerant pressure pulsation signal has weaker electrical noise than the shell surface acceleration signal.

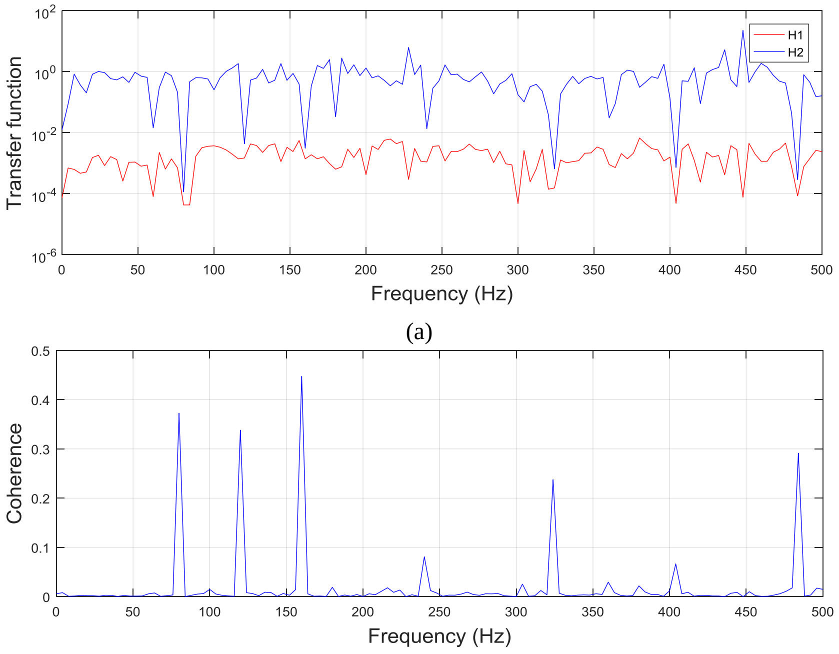

(b)

Fig. 9 Frequency-domain data estimated from the normal compressor: (a) Transfer function; (b) Coherence

3.2 Signal processing

The signals measured from the normal compressor were used to estimate the transfer function and coherence between the refrigerant pressure pulsation signal and shell surface acceleration. The signal of a defective compressor is likely to change in the transfer function according to the type and level of the defect, so the transfer function and the coherence of the normal compressor are more suitable as references for signal processing. The coherence function was applied to the transfer function estimated from the normal compressor to add weight to each frequency. After that, the frequency-weighted acceleration signal was estimated from the shell surface acceleration measured from the defective compressors. The schematic of estimating the frequency-weighted acceleration signal is shown in Fig. 8.

Fig. 9 shows a part of the transfer function and coherence estimated from the data of the normal compressor. In Figs. 9(a) and (b), the space between the transfer functions H_1 and H_2 (that is, the range of the actual transfer function) is relatively small in the frequency band where the coherence is relatively high. The frequency-domain weight was applied to the transfer function using the coherence because the coherence is low at 60 Hz. As a result, the electric noise at 60 Hz can be sufficiently excluded.

Fig. 10 shows a part of the frequency-weighted acceleration signal estimated by weighting the frequency domain of the transfer function from the compressor acceleration signal using Eq. (16).

3.3 Results of defect classification performance

Fisher's discrimination ratio (FDR) was used as an indicator of the defective classification performance of the refrigerant compressors. FDR is useful for simple classifications using the variance and mean. The generalized FDR can be expressed as follows (Attoui *et al*. 2017).

$$\mathrm{FDR}_{\mathrm{M\_class}} = \sum_{i}^{M}\sum_{j\neq i}^{M}\frac{\left(\mu_i-\mu_j\right)^2}{\sigma_i^2+\sigma_j^2} \tag{18}$$

Where σ^2 is the variance, μ is the mean, and M is the number of two or more clusters.

FDR is inversely proportional to the sum of the variances in the cluster and is proportional to the distance between the clusters. This means that the FDR result in better classification of the clusters. The cluster in the discrimination technique consists of a group of representative statistical values of the signals to be discriminated. The proposed fault classification method was evaluated using the frequency center(FC), root-mean-squared frequency (RMSF), and root-variance frequency (RVF). These features are widely used as representative statistical values in the frequency domain and can be expressed as follows (Lei *et al*. 2008).

$$FC = \frac{\int f_i \times s(f_i)df}{\int s(f_i)df} \tag{19}$$

$$RMSF = \sqrt{\frac{\int f_i^2 \times s(f_i)df}{\int s(f_i)df}} \tag{20}$$

$$RVF = \sqrt{\frac{\int (f_i - FC)^2 \times s(f_i)df}{\int s(f_i)df}} \tag{21}$$

where $s(f_i)$ is the PSD function.

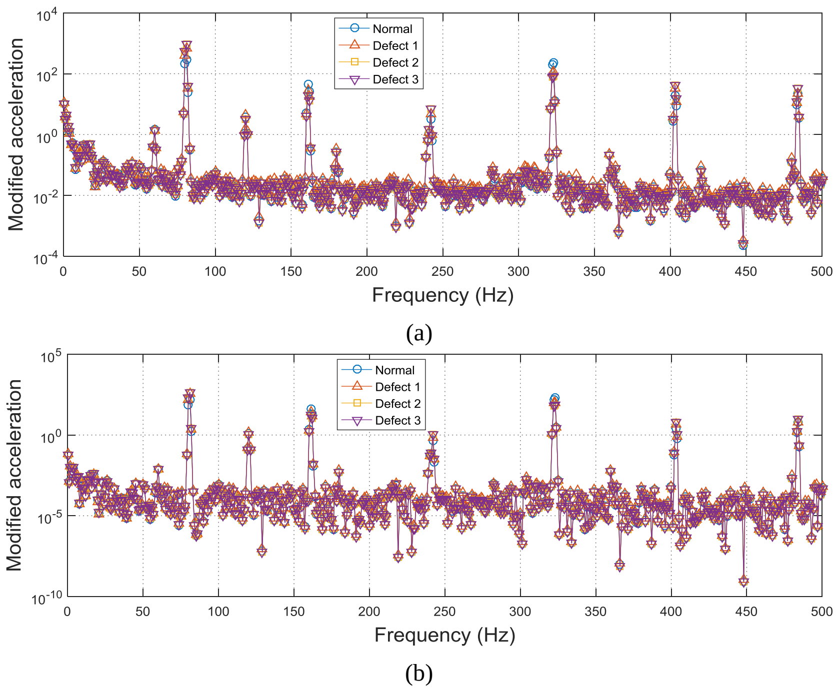

Fig. 10 Frequency weighted acceleration data: (a) Using Transfer function $H_1(f)$; (b) Using transfer function $H_2(f)$

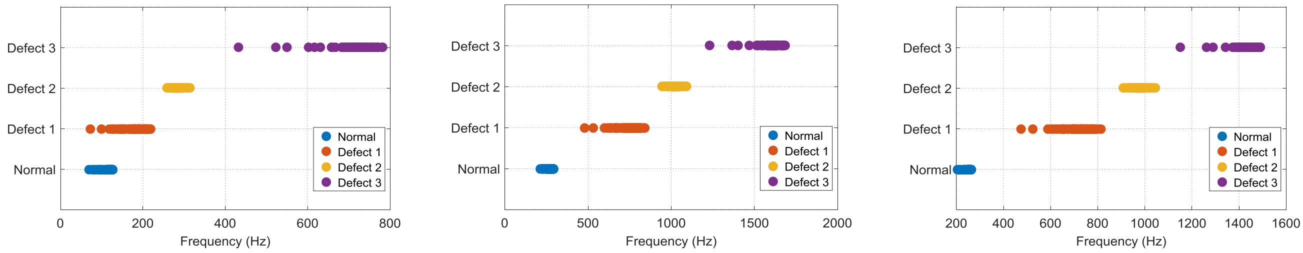

(a) (b) (c)

Fig. 11 Defect classification using only pulsating pressure: (a) FC; (b) RMSF; (c) RVF

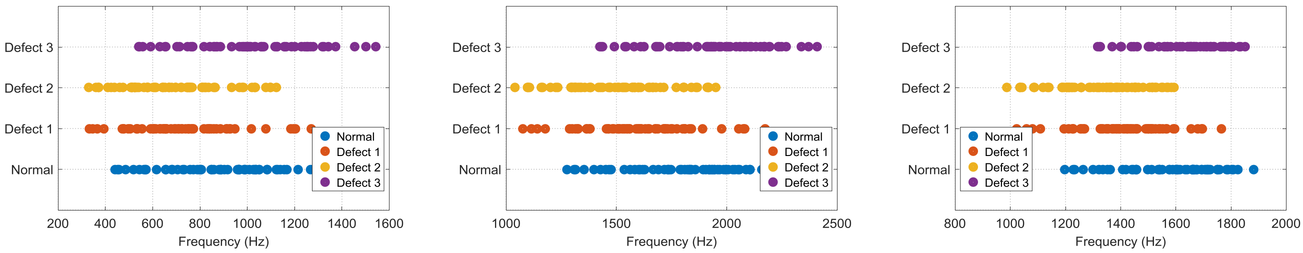

(a) (b) (c)

Fig. 12 Defect classification using only shell acceleration: (a) FC; (b) RMSF; (c) RVF

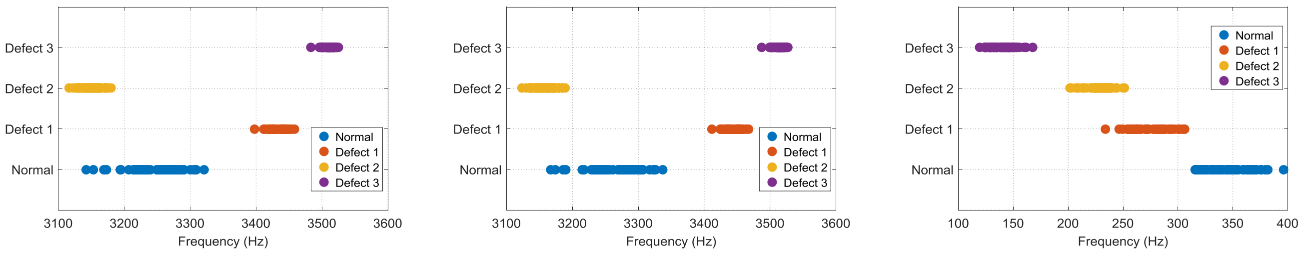

(a) (b) (c)

Fig. 13 Defect classification using modified acceleration signal with $H_1(f)$: (a) FC; (b) RMSF; (c) RVF

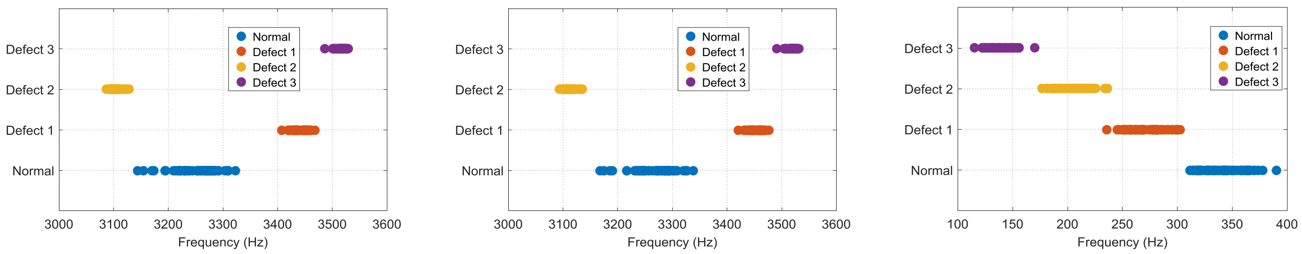

(a) (b) (c)

Fig. 14 Defect classification using modified acceleration signal with $H_2(f)$: (a) FC; (b) RMSF; (c) RVF

Figs. 11 and 12 show the FC, RMSF, and RVF results obtained by dividing the refrigerant pressure pulsation signal and the surface acceleration signal for each type of compressor defect by 60 at intervals of 1 second. The vertical axes show the results of classification of the data measured from the normal compressor and the three kinds of defective compressors. The scale has no meaning.

Fig. 11 shows that the signals of the normal compressor and the defective compressor are well classified by using the RMSF and RVF features. However, it is difficult to measure the pulsation signals in a mass-production line, in contrast to the shell surface acceleration. Fig. 12 shows the classification results of the frequency-domain indexes by directly using the acceleration. All the features are overlapped, and it is difficult to distinguish between the normal compressor and the defective compressor. Therefore, the frequency-domain indexes obtained by directly using the acceleration have almost no classification capability. In addition, the pressure pulsation signal has better classification performance than the shell surface

Table 2 Fisher discrimination ratio of signals

Signal	FC	RMSF	RVF
Pulsating pressure	13	138	206
Shell acceleration	1	2	3
Modified acceleration with $H_1(f)$	287	296	89
Modified acceleration with $H_2(f)$	450	474	94

acceleration signal. Therefore, a signal processing technique is required to use the easily measured acceleration signal.

Figs. 13 and 14 show the results of the proposed classification method using the frequency-weighted acceleration signal. In Figs. 13(a) and (b), some data of the normal compressor and the two defective compressors overlap. In Fig. 13(c), some data of the two defective compressors overlap. Figs. 14(a) and (b) show that all the features are separated from each other. In Fig. 14(c), the data of the two defective compressors are partially overlapped. Compared with Fig. 12(c), the distinction is better. Fig. 14(c) shows a similar trend to the order of "Excess amount of noise compared to manufacturer's standard value" in the Table 1. Fig. 11 shows that the tendency of placement order of the defect feature clusters is similar to that obtained with the classification results using the refrigerant pressure pulsation signal. Compared to Fig. 14, better results were obtained in Fig. 13 by adding the frequency weighting to the transfer function H_2, which minimizes the input noise of the system.

In order to quantitatively evaluate these results, the FDR of each of the classification data was obtained, as shown in Table 2. The defect classification using the refrigerant pressure pulsation signal shows high FDR value in RMSF and RVF. In the case of FC, the FDR is lower than others because the area of the normal compressor and the defect 1 compressor overlap considerably.

The defect classification using the shell surface acceleration directly has very low value compared to that of the other features. This indicates that the shell surface acceleration is also difficult to classify in the FDR index. However, unfortunately, pressure signal is difficult to apply to the defect inspection on production line. Shell acceleration signal which is easy to measure should be used instead of pressure.

Features using the frequency-weighted acceleration signal show higher value than the FDR of the surface acceleration overall. RVF shows relatively low FDR value compared with the classification using the refrigerant pressure pulsation signal, but it shows high FDR value with FC and RMSF. The best performance was obtained using RMSF with transfer function H_2.

4. Conclusions

The pressure pulsation signal of refrigerant is very useful for the quality control of small refrigerant compressors for home use. However, measuring the pressure pulsation signal on a mass-production line takes a long time and is therefore not effective in performing a full inspection. In contrast, the acceleration signal on the shell surface of the compressor is comparatively easy to measure, but the signal containing the structural characteristics of the compressor is measured, so it is not suitable for use in determining the compressor defects. In order to solve these difficulties, this paper proposed a method of using the transfer function between the pressure pulse signal and the acceleration signal. We proposed a signal-processing procedure that improves the defect classification performance of the acceleration signal on the shell surface by weighting the frequency band using the coherence in the process of estimating the transfer function and weighting the frequency band close to the actual transfer function. The method was verified by experiments.

When using raw data without signal processing, the pressure pulsation signal showed high defect classification performance with RVF. However, the defect classification performance was very low when directly using the shell surface acceleration. When applying the proposed signal processing, the defect classification performance was excellent in FC and RMSF overall. In particular, FDR exhibited the best defect classification performance with a value of 474 in the results obtained using transfer function H_2 and RMSF. Using the RVF of the transfer function H_2 showed excellent results except for the fact that there was partial overlap between the results of the two defective compressors.

The transfer function and the coherence between the pressure pulsation and the acceleration signal are measured only once in advance, and only the acceleration signal is measured in the mass-production line. Using the proposed signal processing method makes it easy to classify the compressor defects in a mass-production line and improve the reliability of the product. However, for practical applications, it may be necessary to accumulate more data for normal and faulty compressors.

References

Althobiani, F. and Ball, A. (2014), "An approach to fault diagnosis of reciprocating compressor valves using Teager–Kaiser energy operator and deep belief networks", *Expert Syst. Applica*., **41**(9), 4113-4122. https://doi.org/10.1016/j.eswa.2013.12.026

Aretakis, N. and Mathioudakis, K. (1998), "Classification of radial compressor faults using pattern-recognition techniques", *Control Eng. Practice*, **6**(10), 1217-1223.

Attoui, I., Fergani, N., Boutasseta, N., Oudjani, B. and Deliou, A. (2017), "A new time–frequency method for identification and classification of ball bearing faults", *J. Sound Vib.*, **397**, 241-265. https://doi.org/10.1016/j.jsv.2017.02.041

Bendat, J.S. and Piersol, A.G. (1980), *Engineering Applications of Correlation and Spectral Analysis*, Wiley-Interscience.

Cui, H., Zhang, L., Kang, R. and Lan, X. (2009), "Research on fault diagnosis for reciprocating compressor valve using information entropy and SVM method", *J. Loss Prevent. Process Indust*., **22**(6), 864-867. https://doi.org/10.1016/j.jlp.2009.08.012

Elhaj, M., Gu, F., Ball, A.D., Albarbar, A., Al-Qattan, M. and Naid, A. (2008), "Numerical simulation and experimental study of a two-stage reciprocating compressor for condition monitoring", *Mech. Syst. Signal Process*., **22**(2), 374-389. https://doi.org/10.1016/j.ymssp.2007.08.003

Fan, Y., Nowaczyk, S. and Rögnvaldsson, T. (2015), "Evaluation of self-organized approach for predicting compressor faults in a city bus fleet", *Procedia Comput. Sci.*, **53**, 447-456. https://doi.org/10.1016/j.procs.2015.07.322

Jung, U. and Koh, B.H. (2014), "Bearing fault detection through multiscale wavelet scalogram-based SPC", *Smart Struct. Syst., Int. J.*, **14**(3), 377-395. https://doi.org/10.12989/sss.2014.14.3.377

Kim, Y.W. and Jeong, W.B. (2019), "Modification of acceleration signal to improve classification performance of valve defects in a linear compressor", *Smart Struct. Syst., Int. J.*, **23**(1), 71-79. https://doi.org/10.12989/sss.2019.23.1.071

Kim, M. and Kim, M.S. (2005), "Performance investigation of a variable speed vapor compression system for fault detection and diagnosis", *Int. J. Refrigeration*, **28**(4), 481-488. https://doi.org/10.1016/j.ijrefrig.2004.11.008

Lei, Y., He, Z. and Zi, Y. (2008), "A new approach to intelligent fault diagnosis of rotating machinery", *Expert Syst. Applicat.*, **35**(4), 1593-1600. https://doi.org/10.1016/j.eswa.2007.08.072

Loukopoulos, P., Zolkiewski, G., Bennett, I., Sampath, S., Pilidis, P., Li, X. and Mba, D. (2019), "Abrupt fault remaining useful life estimation using measurements from a reciprocating compressor valve failure", *Mech. Syst. Signal Process.*, **121**, 359-372. https://doi.org/10.1016/j.ymssp.2018.09.033

Mathioudakis, K. and Stamatis, A. (1994), "Compressor fault identification from overall performance data based on adaptive stage stacking", *J. Eng. Gas Turbines Power*, **116**(1), 156-164. https://doi.org/10.1115/1.2906785

Ouadine, A., Mjahed, M., Ayad, H. and El Kari, A. (2018), "Aircraft Air Compressor Bearing Diagnosis Using Discriminant Analysis and Cooperative Genetic Algorithm and Neural Network Approaches", *Appl. Sci.*, **8**(11), 2243. https://doi.org/10.3390/app8112243

Pichler, K., Lughofer, E., Pichler, M., Buchegger, T., Klement, E. P. and Huschenbett, M. (2016), "Fault detection in reciprocating compressor valves under varying load conditions", *Mech. Syst. Signal Process.*, **70**, 104-119. https://doi.org/10.1016/j.ymssp.2015.09.005

Qi, G., Tsai, W.T., Hong, Y., Wang, W., Hou, G. and Zhu, Z. (2016), "Fault-diagnosis for reciprocating compressors using big data", *Proceedings of 2016 IEEE Second International Conference on Big Data Computing Service and Applications*, pp. 72-81.

Qi, G., Zhu, Z., Erqinhu, K., Chen, Y., Chai, Y. and Sun, J. (2018), "Fault-diagnosis for reciprocating compressors using big data and machine learning", *Simul. Model. Pract. Theory*, **80**, 104-127. https://doi.org/10.1016/j.simpat.2017.10.005

Shen, C., Wang, D., Liu, Y., Kong, F. and Tse, P.W. (2014), "Recognition of rolling bearing fault patterns and sizes based on two-layer support vector regression machines", *Smart Struct. Syst., Int. J.*, **13**(3), 453-471. https://doi.org/10.12989/sss.2014.13.3.453

Shin, K. and Hammond, J. (2008), *Fundamentals of Signal Processing for Sound and Vibration Engineers*, John Wiley & Sons.

Tran, V.T., AlThobiani, F., Tinga, T., Ball, A. and Niu, G. (2017), "Single and combined fault diagnosis of reciprocating compressor valves using a hybrid deep belief network", *Proceedings of the Institution of Mechanical Engineers., Part C: J. Mech. Eng. Sci.*, **232**(20), 3767-3780. https://doi.org/10.1177/0954406217740929

Wang, Y., Xue, C., Jia, X. and Peng, X. (2015), "Fault diagnosis of reciprocating compressor valve with the method integrating acoustic emission signal and simulated valve motion", *Mech. Syst. Signal Process.*, **56**, 197-212. https://doi.org/10.1016/j.ymssp.2014.11.002

Yang, B.S., Hwang, W.W., Kim, D.J. and Tan, A.C. (2005), "Condition classification of small reciprocating compressor for refrigerators using artificial neural networks and support vector machines", *Mech. Syst. Signal Process.*, **19**(2), 371-390. https://doi.org/10.1016/j.ymssp.2004.06.002

Zhou, Y., Ma, X. and Yuan, Y. (2006), "Reciprocating compressor fault diagnosis based on vibration signal information entropy", *Mach. Tool Hydraul.*, **10**, 69.

Zhu, D., Feng, Y., Chen, Q. and Cai, J. (2010), "Image recognition technology in rotating machinery fault diagnosis based on artificial immune", *Smart Struct. Syst., Int. J.*, **6**(4), 389-403. https://doi.org/10.12989/sss.2010.6.4.389

FC